

Effect of Si on Fe-rich intermetallic formation and mechanical properties of heat-treated Al–Cu–Mn–Fe alloys

Yuliang Zhao

National Engineering Research Center of Near-Net-Shape Forming for Metallic Materials, South China University of Technology, Guangzhou 510641, China; and School of Engineering & Computer Science, University of Hull, East Yorkshire, HU6 7RX, U.K.

Weiwen Zhang,^{a)} Chao Yang, Datong Zhang, and Zhi Wang

National Engineering Research Center of Near-Net-Shape Forming for Metallic Materials, South China University of Technology, Guangzhou 510641, China

(Received 17 September 2017; accepted 7 November 2017)

The effect of Si on Fe-rich intermetallic formation and the mechanical properties of the heat-treated squeeze cast Al–5.0Cu–0.6Mn–0.7Fe alloy was investigated. Our results show that increasing the Si content promotes the formation of $\text{Al}_{15}(\text{FeMn})_3(\text{SiCu})_2$ (α -Fe) and varies the morphology of T ($\text{Al}_{20}\text{Cu}_3\text{Mn}_2$), where the size decreases and the amount increases. The major reason is that Si promotes heterogeneous nucleation of the intermetallics leading to finer precipitates. Si addition significantly enhances the ultimate tensile strength and yield strength of the alloys. The strengthening effect is mainly owing to the dispersoid strengthening by increasing the volume fraction of the T phase and less harmful α -Fe with a compact structure, which makes it more difficult for the cracks to initiate and propagate during tensile test. The squeeze cast Al–5.0Cu–0.6Mn–0.7Fe alloy with 1.1% Si shows significantly improved mechanical properties than the alloy without Si addition, which has a tensile strength of 386 MPa, yield strength of 280 MPa, and elongation of 8.6%.

I. INTRODUCTION

Al–Cu alloys have been widely used in automobile manufacturing, space technology, and aerospace industry owing to their high specific strength, good heat resistance, and excellent fatigue properties.^{1–3} To meet both recyclable use and increasing demands of Al alloys, recycling Al alloys have become an important source of Al production.^{4–6} For example, the consumption of recovered aluminum in the US in 2015 was ~3.61 million ton, about 46% of which came from old aluminum scrap.⁷ Moreover, production of Al by recycling Al alloys creates only approximately 4% of CO_2 generated by primary production.

As a typical high-strength Al–Cu alloy, the Al–5.0Cu–0.6Mn alloy has wide applications in room and elevated temperatures because of its excellent mechanical properties.⁸ However, one of the greatest challenges to aluminum recycling is the accumulation of impurity elements, such as Fe, Si, Ni, Zn, Mg, and Mn, in recycling of Al alloys, which can cause a sharp degradation in the mechanical properties (ductility, formability, and fatigue properties).^{9,10} Fe is the most common impurity element

in the Al–Cu scrap and is difficult to be eliminated.^{11,12} For high-performance Al–Cu alloys, Fe and Si contents are usually limited to 0.15 and 0.10 wt% (hereinafter weight percentage simply as %), respectively.⁶ Hence, the relatively tolerant limits pose great challenges for direct reuse of these alloys. Since the solid solubility of Fe in Al–Cu casting alloys is limited, Fe atoms usually precipitate in the form of hard and brittle Fe-rich intermetallics, such as Chinese script $\text{Al}_{15}(\text{FeMn})_3(\text{SiCu})_2$ (α -Fe),^{13–20} $\text{Al}_6(\text{FeMn})$,^{19,20} $\text{Al}_m(\text{FeMn})$ ^{18,20} and plate-like $\text{Al}_3(\text{FeMn})$ ^{18,19}, and $\text{Al}_7\text{Cu}_2\text{Fe}$ (β -Fe),^{15,19,20} depending on the alloy composition and cooling rate.

Mn is the most common element added to Al–Cu cast alloys to minimize their harmful influence on the mechanical properties because Mn can transfer the Fe-rich intermetallics from the platelet to the Chinese script.^{14,18–21} It was found that the best Mn/Fe mass ratio is 1.6 (without applied pressure) and 1.2 (at 75 MPa applied pressure), respectively, for the completely converting the needle-like β -Fe phase into the Chinese script Fe-rich intermetallic phases.³¹ It was also reported that Mn addition promotes the transformation of α -Fe, and their transformation efficiency depends on different Fe and Mn contents and cooling rates.^{18,19} It also contributes to the strength of the alloy through solid solution strengthening.²⁰ Usually, 0.4–1.0 wt% Mn is added to the Al–Cu

Contributing Editor: Jürgen Eckert

^{a)}Address all correspondence to this author.

e-mail: mewzhang@scut.edu.cn

DOI: 10.1557/jmr.2017.441

alloys to compensate for the negative effect of Fe.¹⁰ Hence, 0.6% Mn was added into the alloy in the present study.

It is found that the Si/Fe mass ratio has a significant effect on the Fe-rich intermetallics formation.^{13–19} Si can dissolve in the α -Al matrix, excess Si mainly precipitates in the form of Si-containing intermetallics. It has been reported that the addition of $\sim 0.1\%$ Fe and Si results in the solid solution strengthening and impurity hardening of pure aluminum alloys.¹¹ It is found that the combined addition of Mn and Si has a higher transformation efficiency of β -Fe to α -Fe than individual addition of Mn and Si.¹⁴ It is observed that B206 alloys obtained the best mechanical properties when the Si/Fe mass ratio is close to 1 with lower Fe and Si contents.¹⁶ The modification of Fe-rich intermetallic formation can change the mechanical properties, where the α -Fe intermetallic shows a less harmful effect.^{13–16} Minor addition of Si modified the dispersion, morphology, and crystal structure of precipitates of the Al–4Cu–1.3 Mg alloy and an associated increase in tensile strength.¹⁷ Addition of Si in Al–Mg and Al–Mn alloys helps transform the Fe-rich intermetallics from Al₆(FeMn) to α -Fe.^{22–24} Addition of Si to the A201 alloy increased the precipitation of large particles at grain boundaries and in turn enhanced the microhardness of the alloy.²⁴ However, with the increase in Si content, the tensile strength and elongation of T7651 heat-treated 7050 alloys are decreased.²⁵ It is also found that Si addition into Al–Cu catalyzed the precipitation of θ' phases during the aging process.²⁶ However, reports on the best Si additive amount in the alloys are conflicting. Thus, the underlying mechanism still needs to be further investigated.

Heat treatment is one of methods to strengthen Al–Cu alloys with the advantage of dissolution of nonequilibrium phases, elimination of segregation, and formation of high-density fine precipitates. Al–Cu alloys, also called 2XXX series alloy, are one of the most important precipitation-strengthened alloy systems because the precipitation forms age hardening during the heat treatment process.³ The Al₂₀Cu₂Mn₃ (T) phase usually forms within the α -Al matrix of the Al–Cu–Mn alloy after solution treatment and aging, which enhances the high-temperature deformation resistance of the matrix. Except for the precipitates, the Fe-rich intermetallic phases also experience fragmentation and transformed into different Fe-rich intermetallic phases during heat treatment. According to previous studies,^{13,16} α (CuFe) and α -Fe are the two typical Fe-rich intermetallic phases in the heat-treated Al–Cu alloys. α -Fe is usually formed in high-Si-content Al–Cu alloys. Because Si is the only element required for solid solution transformation, Si + Al₆(FeMn) \rightarrow α -Al + α -Fe (called 6- α transformation).²⁷ This reaction needs to intake the Si atom from the α -Al matrix and α -Al from the Fe-rich intermetallic phases.

Squeeze casting combines the features of gravity casting (GC) and plastic processing, which can decrease the casting defects and improve the casting quality.²⁸ Several researchers have reported related studies on the squeeze casting (SC) of Al alloys^{20,29–34} and got satisfied results. A previous study²⁰ shows that the elongation of the Al–Cu–Mn–Fe alloys at 75 MPa applied pressure is two times higher than that of 0 MPa alloys. The optimum SC parameter 2017A wrought Al alloys was revealed: squeeze pressure equal to 90 MPa, melt temperature equal to 700 °C, and die preheating temperature equal to 200 °C.²⁹ The semisolid slurry of the wrought 5052Al alloy and the AlCu5MnTi alloy was prepared by indirect ultrasonic vibration and then shaped by direct SC.^{30,31} They found that the average diameters of the primary α -Al particles decreased with the increase of squeeze pressure as well as increasing the tensile properties of the alloy. A new technology of near liquidus SC can form a globular structure without the preparation of semisolid slurries or billets at a near liquidus pouring temperature.³² The SC techniques can also be used in the preparation of Al-based composite alloys.^{33,34} Stirring followed by SC was used to produce A359 composites containing different weight percentages of (SiC + Si₃N₄) particles.³³ Microstructures of the composites showed a homogeneous and even distribution of hybrid reinforcements within the matrix. The squeeze-cast (SiCp + Ti)/7075 Al hybrid composites have been successfully produced,³⁴ and the tensile strengths of both composites were improved because of the precipitation hardening of the matrix alloy. Hence, SC is an attractive and promising technology for producing Al–Cu alloy components with improved mechanical properties.

Up to now, research on the microstructure evolution and mechanical properties of squeeze cast Al–Cu alloys with high Fe and Si contents during heat treatment is still limited. In the present work, we studied the Fe-rich intermetallic phase and its effect on the mechanical properties of heat-treated Al–5.0Cu–0.6Mn–0.7Fe alloys with the addition of different amounts of Si using SC and GC. Furthermore, the mechanism of Si addition in Al–Cu alloys resulting in the dispersoids strengthening was studied using TEM analysis.

II. MATERIALS AND METHODS

The experimental alloys with different Si contents were produced by melting pure Al (99.5%) and master alloys of Al–50% Cu, Al–10% Mn, Al–20% Si, and Al–5% Fe (from Sichuan Lande High-Tech Industry Company, Changdu, China). According to Ref. 21, the optimum Mn addition is 0.6% to modify the Fe-rich intermetallic phase into a less harmful shape. Fe is the common impurity in Al–Cu alloys, and we focused on high Fe impurity recycled aluminum alloys. Thus, an Fe content of 0.7 wt% was considered in the present work. Different levels of Si content: low

Si-content (Si content: 0 and 1.5%), medium Si-content (Si content: 0.55%), and high Si-content (Si content: 1.1 wt%) were used. Thus, the composition of the designed alloy is Al–5.0Cu–0.6Mn–0.7Fe–*X*Si (*X* = 0, 0.15, 0.55, and 1.1%). The real chemical composition was analyzed by an optical emission spectrometer (Optima 3000, Perkin-Elmer Corporation, Norwalk, Connecticut). The actual compositions of different alloys are Al–5.19Cu–0.64Mn–0.73Fe–0.03Si (alloy 1), Al–5.30Cu–0.63Mn–0.73Fe–0.15Si (alloy 2), Al–5.23Cu–0.63Mn–0.73Fe–0.55Si (alloy 3), Al–5.05Cu–0.67Mn–0.65Fe–1.12Si (alloy 4), respectively. Firstly, 10 kg of raw materials were melted at about 730 °C in a clay-graphite crucible using an electric resistance furnace, and the melts were degassed by 0.5% C₂Cl₆ to minimize the hydrogen content. The pouring temperature was set at 710 °C after degassing, and the die was preheated to approximately 200 °C before SC. After the melt was poured into a cylindrical die, varied pressure (0 and 75 MPa) was applied to the melts and held for 30 s until the melt was completely solidified. Finally, ingots with a size of $\Phi 65 \times 68$ mm were obtained. The samples for T5 heat treatment were solutions treated at 538 °C for 12 h and then quenched into room temperature water. The aging process was performed at 155 °C for 8 h and then the solution was air-cooled.

Tensile samples with the dimensions of $\Phi 10 \times 65$ mm were cut from the edge of the ingots. The tensile test was performed on a SANS CMT5105 standard testing machine with a strain rate of 1 mm/min. At least three samples were tested to obtain the average value. Samples for metallographic observation were cut from the end of the tensile specimens. Then the sample were grinded using different silica papers (100, 1000, 2500 type) and were fully polished. The samples for metallographic observation were etched with 0.5% HF solution for 30 s. Samples for the grain size measurement were examined under a Leica optical microscope with polarized light after anodizing with a 4% HBF₄ solution for about 30 s at 20 V. The volume fractions of Fe-rich intermetallics phases and the area fractions of dispersoids and precipitation-free zone were analyzed with the image analysis software Image-Pro Plus. The measured area fractions of Fe-rich intermetallic phases were transferred as the volume fractions based on the assumption that the morphology of the Fe-rich intermetallic phases is equaled. Nearly 50 different fields were examined for each sample. The average chemical compositions of phases and fracture surfaces of tensile specimens were analyzed using a scanning electron microscope (SEM) (Quanta 200) and an energy-dispersive X-ray analyzer (EDX). In particular, the morphologies of the Fe-rich intermetallic phases and dispersoids were further studied by Tecnai G2 F30, a field emission gun high resolution transmission electron microscopy (TEM) with energy dispersive X-ray (EDX) analysis.

III. RESULTS AND DISCUSSION

A. Microstructure

Figure 1 shows the as-cast and heat-treated microstructures of the Al–5.0Cu–0.6Mn–0.7Fe alloys with different Si contents and applied pressure. The as-cast alloys usually consisted of the α -Al matrix, Fe-rich intermetallic phases, and Al₂Cu. The black Al₆(FeMn), deep gray α -Fe, and light gray Al₂Cu can be seen in the matrix in the as-cast alloy 1, as shown in Fig. 1(a). Figure 1(b) shows the deep gray α -Fe and light gray Al₂Cu existed in the as-cast alloy 4, which indicates that the size and amount of α -Fe increased with the increase of the Si content. The heat-treated alloys consisted of the α -Al matrix, Fe-rich intermetallic phases. The Al₂Cu dissolved into the α -Al matrix during the T5 heat treatment, as shown in Figs. 1(c)–1(f). The results show that Si addition promotes the transformation from α (CuFe) (the composition is the same as the as-cast state β -Al₇Cu₂Fe) to α -Fe at the heat treatment state. α (CuFe) and Al₆(FeMn) are the dominant Fe-rich intermetallics at low Si contents as shown in Fig. 1(c). With the Si content increased to 0.15%, the Al₆(FeMn) gradually transformed into α -Fe [Fig. 1(d)], while a small volume percentage of fine Al₆(FeMn) remained. These results are also consistent with a previous finding²¹ that Si addition promotes the formation of α -Fe due to the substitution of the Al atom by the Si atom in Fe-rich intermetallic phases. After the addition of 0.55% Si, Al₆(FeMn) and α -Fe existed in alloy 3 (containing 0.5% Si), while the amount of α -Fe sharply increased and a small amount of Al₆(FeMn) still remained [Fig. 1(e)]. Further increasing the addition level of Si to 1.1%, α -Fe was the only Fe-rich intermetallic phase in alloy 4 as shown in Fig. 1(f). The effect of applied pressure on the Fe-rich intermetallic phases of alloys is shown in Figs. 1(g) and 1(h). Compared to alloy 1 without applied pressure [Fig. 1(c)], the sizes of α (CuFe) and Al₆(FeMn) become relatively smaller [Fig. 1(g)]. Similarly, the size of α -Fe in the alloy with 75 MPa applied pressure became smaller and the branches of α -Fe became disconnected and closed to semi-circle shape [Fig. 1(h)]. This indicates that applied pressure could relatively refine the Fe-rich intermetallic phases. The volume percentage of α -Al, α (CuFe), Al₆(FeMn), and α -Fe with different Si contents and applied pressure has been measured as shown in Fig. 2. This further indicates that Si addition promotes the formation of α -Fe in the heat treatment state. Moreover, the total volume percentage of Fe-rich intermetallic phases under 75 MPa applied pressure is smaller than that of those without the applied pressure. This is similar to Refs. 20 and 21 because the solubility of Cu and Mn is more in the α -Al matrix under applied pressure. The composition of Fe-rich intermetallic phases in the as-cast and heat treatment state is given in Table I. It can be seen that

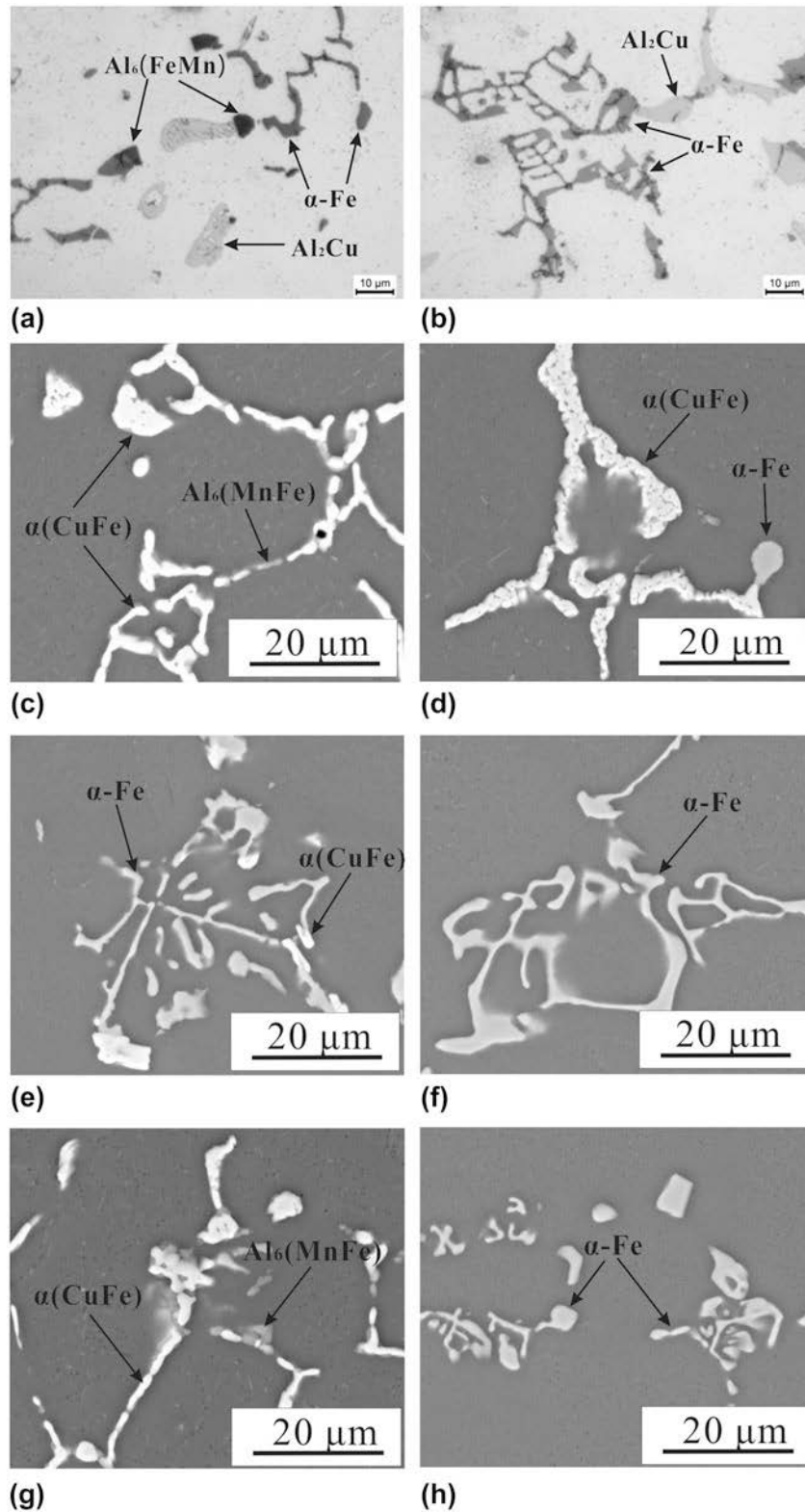


FIG. 1. Microstructure of the Al–Cu–Mn alloys with different Si contents and applied pressure: (a) as-cast alloy 1 without applied pressure; (b) as-cast alloy 4 without applied pressure; (c) heat-treated alloy 1 without applied pressure; (d) heat-treated alloy 2 without applied pressure; (e) heat-treated alloy 3 without applied pressure; (f) heat-treated alloy 4 without applied pressure; (g) heat-treated alloy 1 with 75 MPa applied pressure; (h) heat-treated alloy 4 with 75 MPa applied pressure.

the Cu content in heat-treated $\alpha(\text{CuFe})$ is much higher than in the as-cast $\text{Al}_3(\text{FeMn})$ and $\text{Al}_6(\text{FeMn})$, and Si, Cu, and Mn content in heat-treated alloys is relatively higher than in as-cast alloys. This indicates that Fe-rich intermetallic phases experience solid-state transformation during heat treatment.

Figure 3 shows the effect of applied pressure on the grain size of alloys and 3D morphology of Fe-rich intermetallic phases. Figures 3(a) and 3(b) show the grain size distributions of the alloy 1 with and without applied pressure, respectively. It can be seen that the grain size of alloy with 75 MPa applied pressure ($\sim 300 \mu\text{m}$) is much smaller than that of the alloy without applied pressure ($\sim 510 \mu\text{m}$). The grain refinement effect is mainly attributed to the increase in the melting point of alloy and the heat-transfer rates between the casting and die interface by eliminating air gaps.²⁴ Figures 3(c)–3(f) presents the deep-etched images of heat-treated Fe-rich intermetallic phases in alloys with different Si content and applied pressure. It can be observed that the $\alpha(\text{CuFe})$ phase in alloy 1 has a cylindrical shape, as indicated in Fig. 3(c). The convoluted branched structure $\alpha\text{-Fe}$ in alloy 4, which is a coupled eutectic product, grows from the large convoluted arm structure and $\alpha\text{-Al}$ dendrite,³⁵ as shown in Fig. 3(d). Compared with Figs. 3(c) and 3(d), the size of Fe-rich intermetallic phases [Figs. 3(e) and 3(f)] in the alloy produced under 75 MPa applied pressure becomes smaller.

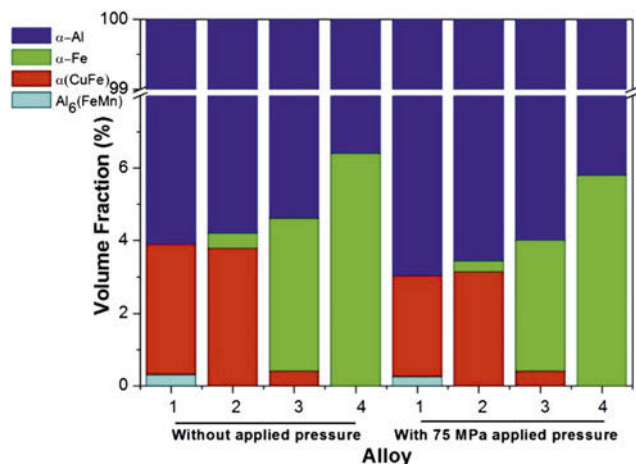


FIG. 2. The volume percentage of different phases in the heat-treated alloys under different applied pressures.

These results are consistent with the microstructure features (Fig. 1). Thus, the applied pressure can not only refine the $\alpha\text{-Al}$ but also the Fe-rich intermetallic phases.

Figure 4 shows the TEM analysis of Fe-rich intermetallic phases in the alloy 1 and 4. From the selected area diffraction pattern (SADP) shown in Fig. 4(a), the A phase is identified as $\text{Al}_6(\text{FeMn})$, which has an orthorhombic crystal structure with lattice constants of $a = 0.643 \text{ nm}$, $b = 0.746 \text{ nm}$, and $c = 0.878 \text{ nm}$. The SADP result of the B phase also confirms the crystal structure of $\alpha(\text{CuFe})$, which has a tetragonal structure with lattice constants of $a = b = 0.634 \text{ nm}$ and $c = 1.488 \text{ nm}$. The chemical composition of $\alpha(\text{CuFe})$ is close to the as-cast state phase $\beta\text{-Fe}$. Figures 4(b) and 4(c) shows the TEM images of the $\alpha\text{-Fe}$ in the alloy 4. Figure 4(b) is a typical high-resolution TEM image, indicating that the $\alpha\text{-Fe}$ (alloy 4) has the body-centered cubic (BCC) structure with a lattice constant of $a = 1.267 \text{ nm}$. This is further confirmed in the HRTEM image in Fig. 4(c).

Besides the Fe-rich intermetallic phases, a dense distribution of T ($\text{Al}_{20}\text{Cu}_3\text{Mn}_2$) phase dispersoids in $\alpha\text{-Al}$ matrix is shown in Figs. 5(a)–5(d). It can be further confirmed by the indexed SADP and TEM micrographs as shown in Figs. 5(e)–5(h). It can be seen from Figs. 5(a)–5(d) that the size of the dispersoids decreased significantly, while their quantity increased rapidly with increasing Si content, especially for the alloys under applied pressure. A few precipitates can also be found in the intragranular regions [Fig. 5(e)]. The interface between $\alpha\text{-Al}$ and the T phase [as the red circle shown in Fig. 5(e)] has been analyzed by high-resolution electron microscopy (HREM) images, as shown in Fig. 5(f). The precipitates and $\alpha\text{-Al}$ are further identified by SADP, as shown in Figs. 5(f) and 5(g). The composition of the T phase is Al: 79.21%, Mn: 12.17%, Cu: 7.40% and Fe: 1.21% [Fig. 5(h)]. There are several possible explanations for the effect of addition of Si content on enhancing the T precipitation. First, Si may provide nuclei for the heterogeneous nucleation and retard the coarsening of the precipitates. The presence of Si in the alloy reduces the solubility of Mn in the $\alpha\text{-Al}$ matrix,³⁶ thereby increasing the chemical driving force for the T phase precipitation and reducing the $\alpha\text{-Al}/\text{T}$ interfacial free energy. Moreover, the aspect ratio of the T phase decreases with the increase of Si content, which means that Si addition increases the coarsening resistance of precipitates in the T phases. The high number density of

TABLE I. Chemical composition of the Fe-rich intermetallics in the as-cast and heat-treated conditions (at.%).

Conditions	Alloys	Phase	Al	Cu	Mn	Fe	Si
As-cast	1	$\text{Al}_6(\text{FeMn})$	80.05 ± 1.78	5.12 ± 0.85	2.64 ± 0.34	12.19 ± 1.91	...
	4	$\alpha\text{-Fe}$	73.45 ± 0.85	1.98 ± 0.35	3.02 ± 0.60	9.89 ± 0.24	8.90 ± 0.55
	1	$\text{Al}_6(\text{FeMn})$	85.36 ± 1.67	3.08 ± 0.31	2.76 ± 0.22	8.79 ± 1.21	...
Heat-treated	1	$\alpha(\text{CuFe})$	61.95 ± 1.77	22.10 ± 1.08	2.53 ± 0.49	13.41 ± 0.89	...
	4	$\alpha\text{-Fe}$	71.69 ± 1.93	3.71 ± 0.28	5.04 ± 0.49	9.54 ± 0.90	10.12 ± 0.77

the T phase precipitates is responsible for explaining the small size and low aspect ratio. Si and precipitates in alloys have a strong elastic interaction because of their compensating strain fields, which promotes the nucleation of the precipitates on Si, decreases the expected aspect ratio of precipitates, and inhibits coarsening. Also, Si addition increases the attractive binding energy between Si and the vacancy, which can act as heterogeneous nucleation sites for dispersoid T phases.³⁷ Moreover, high diffusivity of Si in the α -Al matrix can accelerate the diffusion kinetics of the elements Cu and Mn and reduce the T phase precipitate coarsening resistance.²⁷

The schematic image of the microstructure evolution in alloys with different Si contents is shown in Fig. 6. After the alloys underwent solid-state treatment at 538 °C for 12 h, the entire amount of Al_2Cu is dissolved into the Al matrix, as shown in Figs. 1(c)–1(h). During the solid-state treatment, the Fe-rich intermetallic phases become unstable and fragmented and are transformed into newly different Fe-rich intermetallic phases. Compared to the morphology of the as-cast Fe-rich intermetallic phases [Figs. 1(a) and 1(b)], no significant change of the morphology of the Fe-rich intermetallic phases has occurred during the heat treatment, except that some

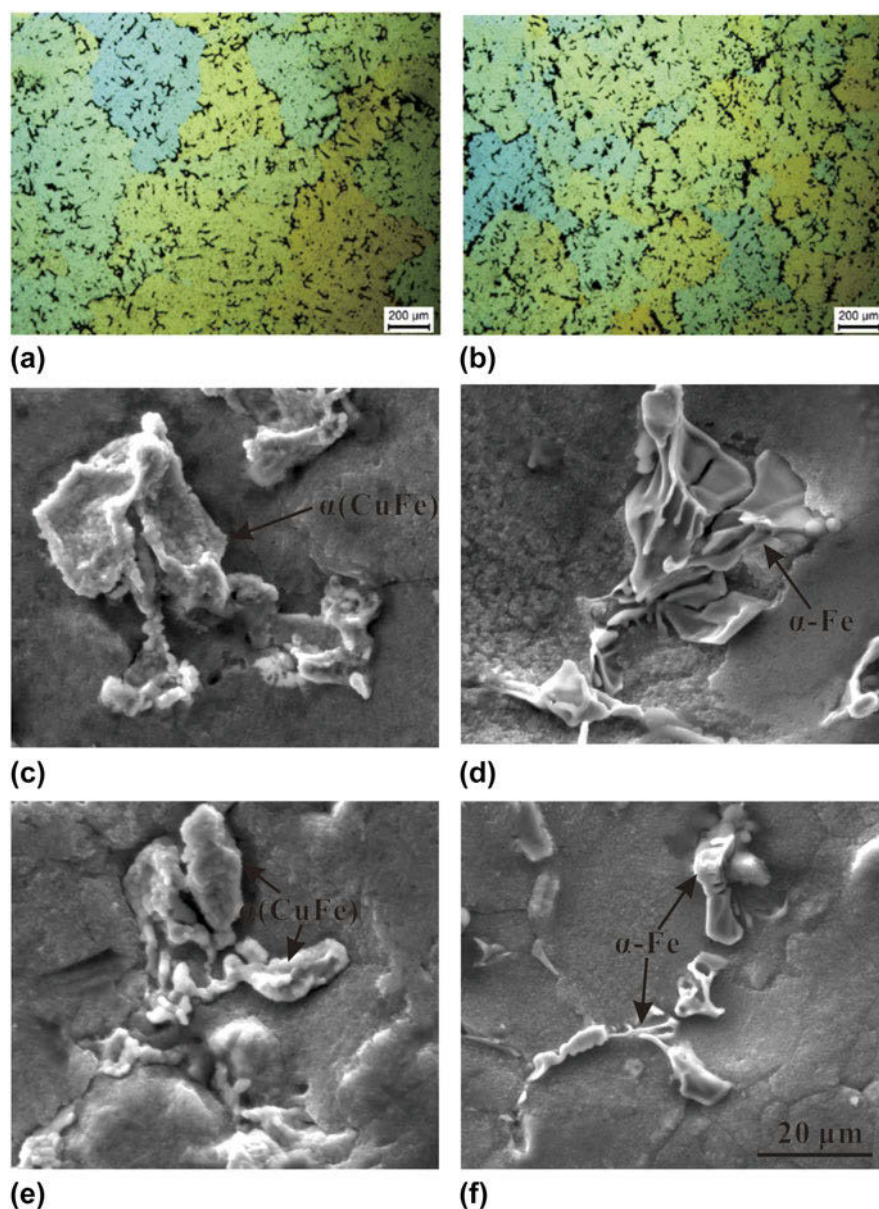
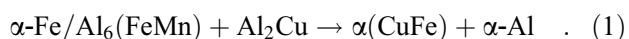


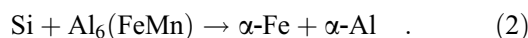
FIG. 3. Effect of applied pressure on the grain size: (a) alloy 1 without applied pressure and (b) alloy 1 with 75 MPa applied pressure; 3D morphology of Fe-rich intermetallics of heat-treated alloys: (c) heat-treated alloy 1 without applied pressure; (d) heat-treated alloy 4 without applied pressure; (e) heat-treated alloy 1 with 75 MPa applied pressure; (f) heat-treated alloy 4 with 75 MPa applied pressure.

Fe-rich intermetallic phases become less connected. In the low Si alloy (alloy 1 and 2), $\alpha(\text{CuFe})$ nucleates on the interface between $\alpha\text{-Fe}/\text{Al}_6(\text{FeMn})$ and the $\alpha\text{-Al}$ matrix [Fig. 4(a)] as well as the Cu atoms diffuse into $\alpha\text{-Fe}/\text{Al}_6(\text{FeMn})$ during the heat treatment, as shown in Figs. 6(a)–6(d) because of the high density of dislocations on the interface of $\alpha\text{-Fe}/\text{Al}_6(\text{FeMn})$ and the $\alpha\text{-Al}$ matrix. Once $\alpha(\text{CuFe})$ nucleates, it will quickly grow in a manner of dendritic growth. This is can be attributed to the relatively high diffusion rate of Cu and Mn at 538 °C. These results are similar to the results in Ref. 21. In addition, a small amount of $\text{Al}_6(\text{FeMn})$ remained in the alloy due to lack of sufficient Cu to form $\alpha(\text{CuFe})$. Thus, the solid-state transformation of the alloy 1 and 2 is a eutectoid reaction:



In high-Si-containing alloys (alloy 3), the dominant $\alpha\text{-Fe}$ and a small amount of $\alpha(\text{CuFe})$ are distributed in the matrix. On the other hand, there is only $\alpha\text{-Fe}$ in alloy 4,

indicating the occurrence of the eutectoid reaction with increasing Si content:



$\alpha\text{-Fe}$ usually nucleates on the interface between the $\text{Al}_6(\text{FeMn})$ and $\alpha\text{-Al}$ matrix and consumes the $\text{Al}_6(\text{FeMn})$ progressively [Figs. 6(e)–6(h)]. The phase transformation from $\text{Al}_6(\text{FeMn})$ to $\alpha\text{-Fe}$ is called “6-to- α transformation”, and Si is the key factor for this transformation.^{27,36–38} The free Si atom diffuses into $\text{Al}_6(\text{FeMn})$ and decomposes into a mixture of $\alpha\text{-Fe}$ and $\alpha\text{-Al}$. The decomposition of $\text{Al}_6(\text{FeMn})$ preserves the volume and content of Fe and Mn and the required intake of Si. If there are more free Si atoms in the surrounding $\alpha\text{-Al}$ matrix, the rate of “6-to- α transformation” increases. The diffusion coefficient of Si in $\alpha\text{-Al}$ at 500 °C is about $1.4 \times 10^{-13} \text{ m}^2/\text{s}$,³³ which is much higher than that of Cu and Mn. Si in the matrix diffuses into $\text{Al}_6(\text{FeMn})$, which accelerates the eutectoid reaction. With the increase of Si content, the volume percentage of $\alpha\text{-Fe}$ increases in alloy 3. For alloy 4, $\alpha\text{-Fe}$ is thermodynamically stable because

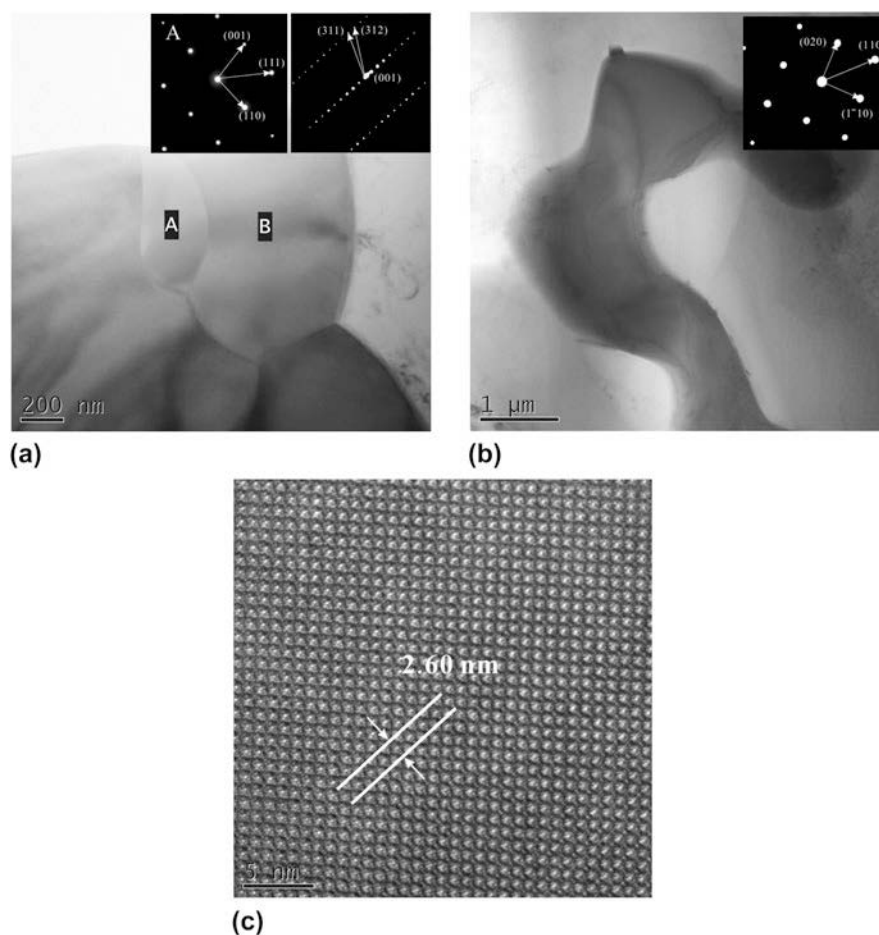


FIG. 4. TEM analysis of the Fe-rich intermetallics: (a) bright-field image of $\text{Al}_6(\text{FeMn})$ and $\alpha(\text{CuFe})$ and the corresponding SAED pattern in alloy 1; (b) TEM image of $\alpha\text{-Fe}$ and the corresponding SAED pattern in alloy 4; (c) the HRTEM image of $\alpha\text{-Fe}$.

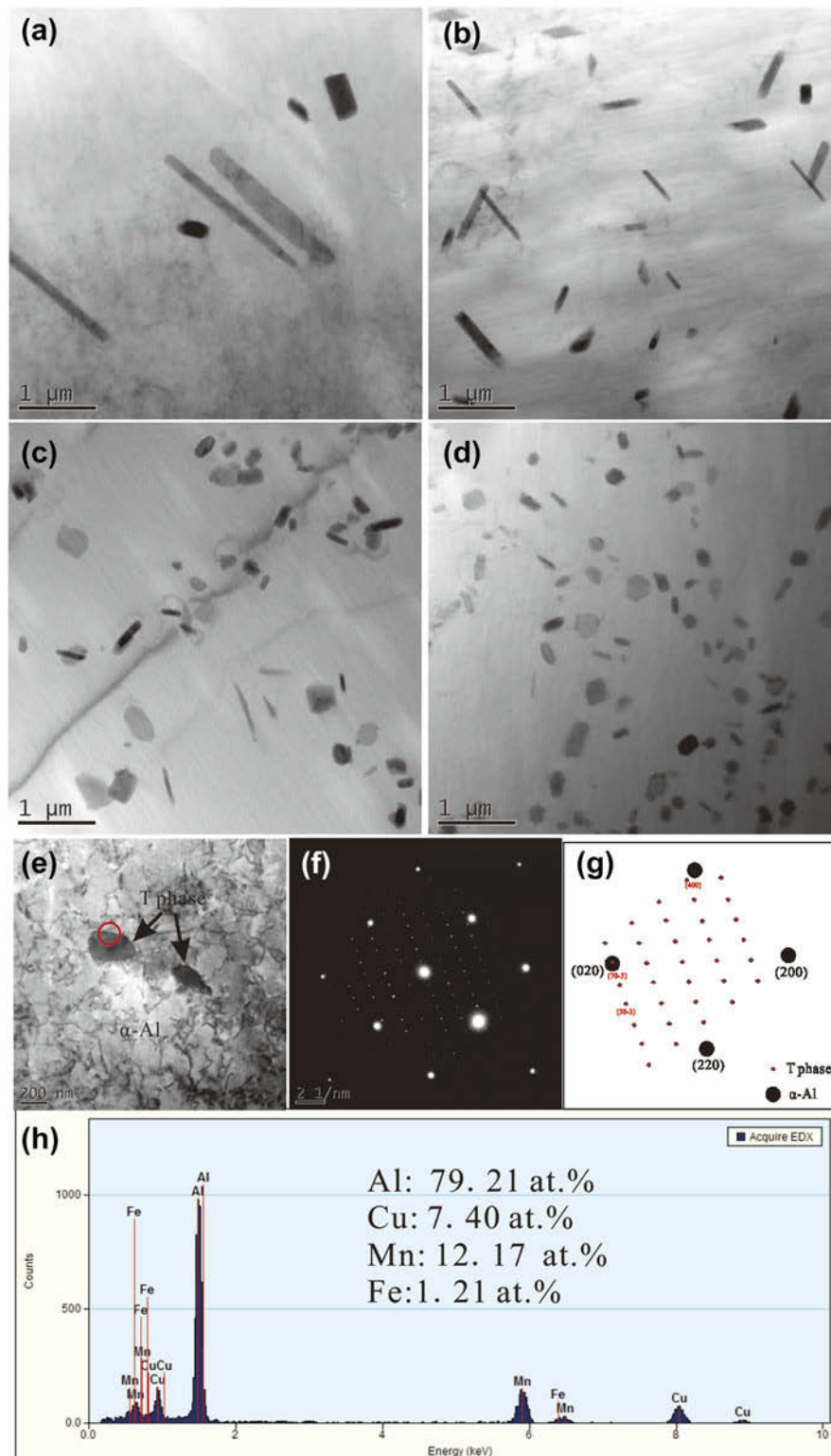


FIG. 5. TEM images showing the morphology and density of T phase dispersoids in heat-treated alloys: (a) alloy 1 without applied pressure; (b) alloy 1 with 75 MPa applied pressure; (c) alloy 4 without applied pressure; (d) alloy 4 with 75 MPa applied pressure; (e) T phase in the matrix of alloy 1; (f, g) SADP of T phase/matrix interfaces and their schematic diagram; (h) the chemical composition of the T phase.

Si is the key element for the α -Fe.^{27,38} With the increase of the Si atom in the α -Al matrix, the thermodynamically stable phase changes from $Al_6(FeMn)$ to α -Fe. Previous studies³⁸ also confirmed this; the nucleation of the α -Fe phase is the overall rate-controlling factor for the 6-to- α transformation. If a greater source of silicon could be supplied in the alloys, the growth of the α -phase-Al eutectoid through a particle is relatively fast. Moreover, Si promotes thermodynamically stable α -Fe and prevents the transformation of α -Fe to $\alpha(CuFe)$ because Si can substitute Al and Si can substitute Cu in α -Fe.

B. Mechanical properties

The effect of Si content on the mechanical properties of heat-treated Al–5.0Cu–0.6Mn–0.7Fe alloys is shown in Fig. 7. There is a considerable increment in the ultimate tensile strength (UTS) and the yield strength (YS), but a significant decrement in the elongation in alloys with increasing the Si contents from 0 to 1.1%. For example, compared with alloy 1 (0% Si), UTS and YS of alloy 4 (1.1% Si) without applied pressure were 29.7% and 101.5% higher than those of alloy 1, respectively. It can also be seen that the applied pressure improved the mechanical properties of the alloys. The UTS, YS, and elongation of the squeeze-cast Al–5.0Cu–0.6Mn–0.7Fe–1.1Si alloys are 386 MPa, 280 MPa, and 8.6%, respectively, which are about 21.2%, 6.9%, and 73.9%, respectively, higher than those of

the alloy without applied pressure. In addition, the Si particles in the high-Si-content alloys (alloy 4) also benefit the improvement of strength. According to a previous study,³⁹ a small Si peak could be found in the XRD analysis although the Si particles could not be found in the SEM images, which may be owing to the similar atomic weights of Al and Si.

Table II summarizes the mechanical properties of Al–Cu alloys with various Fe and Si contents as found in the literature^{13,16,21,40,41} and the present study. These alloys are prepared by different techniques, including GC, SC, and high-pressure die casting (HPDC), and their alloy composition focused on the low Fe and Si impurities content. Reference 21 reported a high-impurity Fe content in the Al–5.0Cu–0.6Mn–1.0Fe alloy, while their tensile properties (UTS and elongation) were not very good. The UTS values of the Al–Cu alloys reported by Refs. 13 and 16 are relatively high, while their elongation values are relatively low. The HPDC-processed Al–4.4Cu–0.2Fe–1.2Si–0.4Mg–0.2Ti alloys⁴¹ possess excellent tensile properties (combined UTS and elongation), while their Fe impurity content is relatively low that it is not suitable for recycled alloys. It can be seen that alloy 4 (containing high Fe and Si impurities) possesses combined high strength and high ductility. In this regard, the SC technique can relatively extend the Fe and Si limitation in the Al alloys. Moreover, the mechanical properties of alloy 4 meet the requirements of the safety-critical suspension component in the

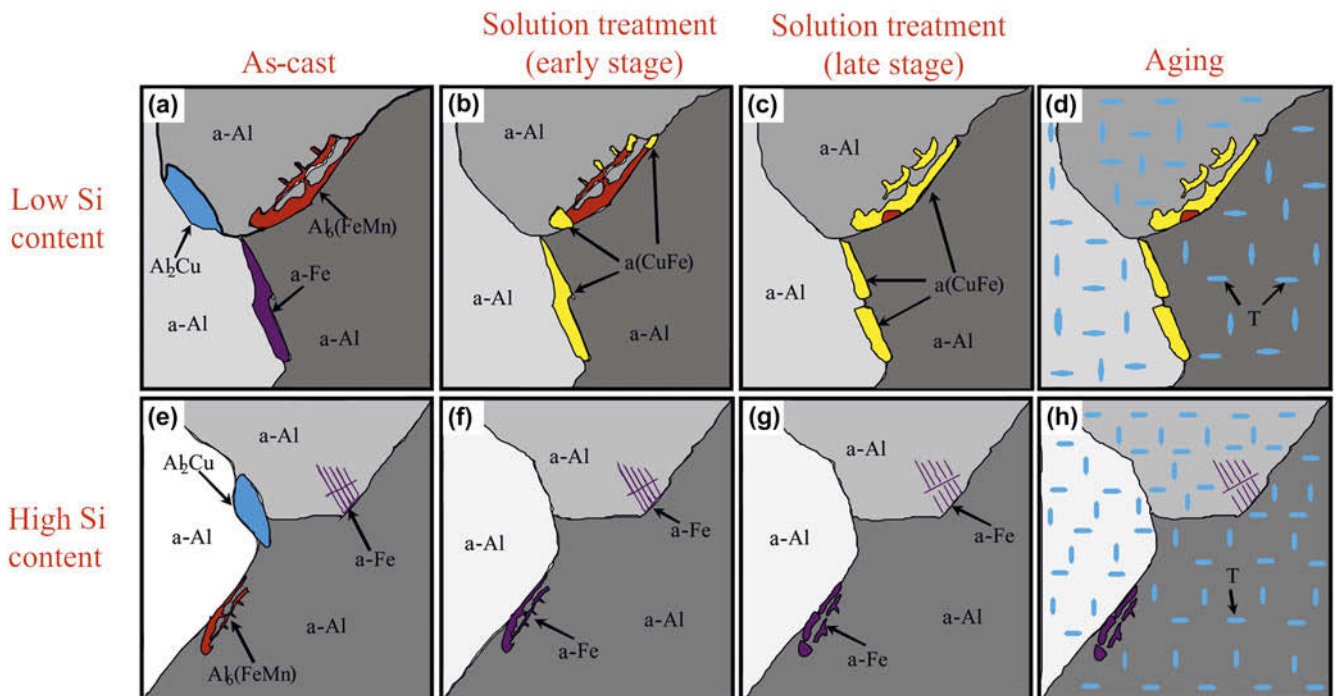


FIG. 6. Schematics of the microstructure evolution of alloys with different Si contents: (a–d) low-Si-content alloys; (e–h) high-Si-content alloys; (a, e) the as-cast alloys; (b, f) solution treatment, early stage: the dissolution of Al_2Cu phase; (c, g) solution treatment, late stage: the fragmentation of Fe-rich intermetallic phases; (d, h) aging: precipitation fine T phases.

automotive industry (UTS > 380 MPa and elongation > 7%). This means that the present study is helpful to promote recycled aluminum alloys for their high-efficiency utilization and lowering the manufacture cost.

To further evaluate the mechanical properties, quality index (QI) was used to characterize the casting quality. QI was firstly introduced by Cáceres et al.^{42,43}. This index is obtained according to the variation of UTS with the elongation obtained with alloys submitted to different metal treatments, heat treatments, or alloy compositions. The QI of the studied alloys can be calculated by the following equation⁴²:

$$QI = UTS + d \log El \quad (3)$$

where QI stand for quality index, UTS and El stand for ultimate tensile strength and elongation, respectively, and

d is an empirically determined constant (we take 270 for d in the present study). It is found that the QI value of alloy 4 without applied pressure is 522 MPa, while that of alloy 4 with the applied pressure of 75 MPa is 656 MPa. Due to the higher UTS and elongation, the QI value of alloy 4 increases with increasing applied pressure. In addition, the QI value varies with different chemical compositions, such as Si content. It is found that the QI value of alloy 1 without applied pressure is 531 MPa, while it is 522 MPa for alloy 4. Nevertheless, the QI value of alloys varies with increasing Si content at the same level of applied pressures. Overall, the applied pressure is helpful to improve the QI and increasing Si content keep QI value at the similar level. Consequently, the Si content limitation can be relatively relaxed under applied pressure. The best QI value of 656 MPa obtained in this study was for alloy 4 with the applied pressure of

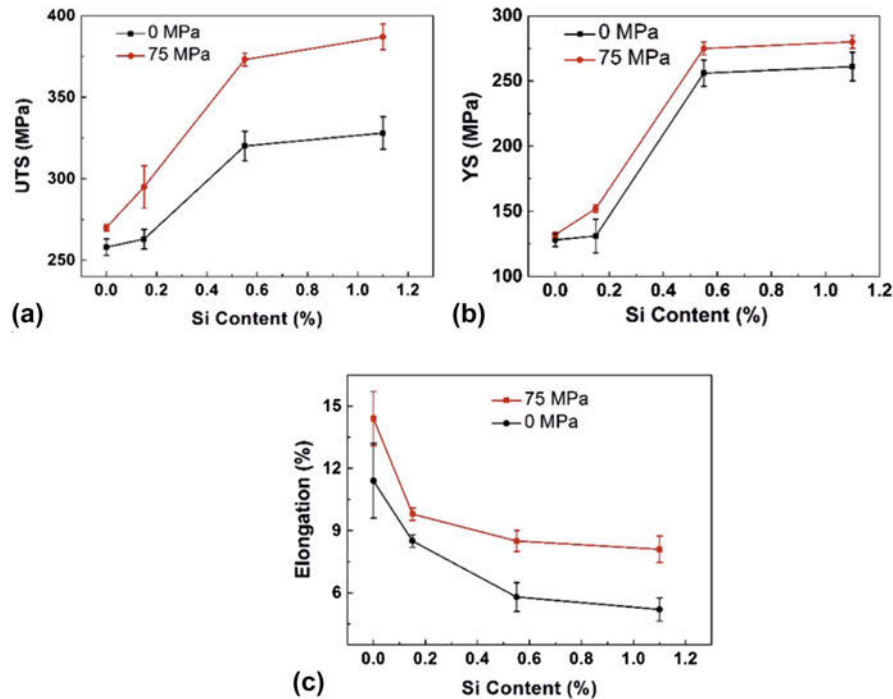


FIG. 7. Effect of Si content on the mechanical properties of heat-treated Al–5.0Cu–0.6Mn–0.7Fe alloys: (a) UTS, (b) YS, and (c) elongation.

TABLE II. Mechanical properties of Al–Cu alloys based on the literature and the present study.

Alloy	Processing ^a	Heat treatment ^b	UTS (MPa)	Elongation (%)	Reference
Al–5.0Cu–0.6Mn–1.0Fe	GC	T5	250	5.5	40
Al–5.0Cu–0.6Mn–1.0Fe	SC	T5	290	14	40
Al–4.6Cu–0.3Mn–0.5Fe–0.3Mg–0.3Si–0.2Ti	GC	T7	424	2.8	13
Al–4.7Cu–0.2Mn–0.3Fe–0.3Si–0.3Mg	GC	T7	510	1.5	16
Al–4.4Cu–0.2Fe–1.2Si–0.4Mg–0.2Ti–1.2Si	HPDC	T7	370	9	41
Al–5.0Cu–0.7Fe–0.6Mn–1.1Si	SC	T5	386	8.6	Present study

^aGC—gravity casting, SC—squeeze casting, HPDC—high-pressure die casting.

^bHeat treatment: T4: solution treatment at 505 °C/2 h + 520 °C/8 h + aging at room temperature/8 d; T5: solid state: 538 °C 12 h + aging: 155 °C 8 h; T7: solid state: 505 °C 2 h + 520 °C 8 h + aging: 185 °C 5 h.

75 MPa. Kamga et al.¹⁶ reported B206 (a kind of typical Al–Cu–Mn) alloys with low Fe and Si content (0.1–0.3%) under T4 and T7 heat treatment. They found that when the Fe/Si ratio is close to one and with a high cooling rate, high mechanical properties are obtained. Their QI values were in the range of 557–640 MPa for T7 heat treatment and 727–810 MPa for T4 heat treatment. It can be seen that natural aging (T4 heat treatment) can result in higher QI values because of the higher elongation. A previous study¹⁶ has reported a higher QI value than that of the present study because of the low Fe and Si content in the B206 alloys (up to 0.3%). Thus, to obtain a good casting quality and high QI value, we should take the alloy composition, heat treatment, and cooling rate into consideration.

The above tensile testing show that Si addition enhances the strength of the alloys. The main reason for this is that the volume percentage of α -Fe increases while the volume percentage of α (CuFe) decreases (Fig. 2) and the T phases increases with increasing Si content (Fig. 5). α -Fe is less harmful than α (CuFe) because the Chinese script α -Fe has a compact structure, which makes it more difficult for the cracks to initiate and propagate during the tensile test. Usually, α -Fe has well-developed branches in different directions; they mutually interweave with the Al matrix.¹³ During the tensile test, the refined α -Fe branches block the crack propagation, and it only can propagate along the α -Fe/matrix interface. Also, the void cannot easily be developed around α -Fe. Another factor is mainly attributed to the dispersoid strengthening in the matrix. The amount of the T phase in the matrix increases and the size decreases with the increasing Si content during the T5 heat treatment. The yield strength of alloys (σ) is usually composed of three parts: the strength of dispersoid strengthening (σ_D), the strength of solid solution strengthening (σ_{SS}), and the strength of α -Al matrix (σ_{Al}).⁴⁴

$$\sigma = \sigma_D + \sigma_{SS} + \sigma_{Al} \quad (4)$$

In the present work, the T phase dispersoid strengthening in the matrix and solid solution strengthening both contribute to the improvement of the strength. For example, with the Si content increasing from 0 to 1.1% without applied pressure [Table III and Figs. 5(a) and 5(c)], the incensement of strength is 12.98 MPa. This can be attributed to the solid solution strengthening of Si

addition. A large number of fine precipitates in the matrix pose a hindrance to moving dislocations resulting in the enhancement of strength. And the strength of the α -Al matrix is 5.14 MPa. The solid solution strengthening mainly depends on the concentration of the solute in the solid solution, while the Fe, Si, Mn, and Cu solute atoms in Al–Cu alloys dissolve into the matrix contributing to the improvement of the strength. Because of the low solubility of Fe and Si in the matrix, their solid solution strengthening contribution to the improvement of strength can be neglected. According to Ref. 40, the solid solution of Cu and Mn in Al–5.0Cu–0.6Mn–1.0Fe is increased with the improvement of the applied pressure. For alloy 1, with the applied pressure increasing from 0 to 75 MPa [Table III and Figs. 5(a) and 5(b)], the incensement of strength is 2.06 MPa. Because the size of the dispersoids in the T phase is relatively large, the Orowan mechanism can be applied in the present study. The contribution of dispersoid strengthening can be calculated by the Ashby–Orowan equation^{44,45}:

$$\sigma_D = \frac{0.84MGb}{2\pi(1-\nu)^{1/2}\lambda} \ln \frac{r}{b} \quad (5)$$

where M is the Taylor factor, $M = 3.06$; G is shear modulus of the Al matrix, $G = 27.4$ GPa; b is the Burgers vector of dislocation in Al, $b = 0.286$ nm; and ν is the Poisson ratio, $\nu = 0.33$ for Al. The interspacing of dispersoids λ depends on the radius r and the volume fraction f of dispersoids⁴⁶:

$$\lambda = r \left(\frac{2\pi}{3f} \right)^{1/2} \quad (6)$$

The parameters for calculating the dispersoid strengthening of the alloys and the calculated dispersoid strengthening σ_D are listed in Table III. In alloys with 0 and 1.1% Si content without applied pressure, the equivalent diameter of the T phase is 1.07 and 0.33 μm , respectively, and their corresponding number density is about $5.75 \times 10^{20} \text{ m}^{-3}$ and $48 \times 10^{20} \text{ m}^{-3}$, respectively; their corresponding dispersoid strengthening is about 5.14 MPa and 18.12 MPa, respectively. It can be found that the equivalent diameter of the T phase decreases by

TABLE III. The parameter for calculation of the dispersoid strengthening of the alloys.

Alloys	Applied pressure (MPa)	Equivalent diameter D (μm)	Volume fraction f (%)	Number density (10^{20} m^{-3})	Volume fraction of dispersoids zone (%)	Volume fraction of dispersoids free zone (%)	σ_D (MPa)
1	0	1.07	1.76	5.75	2.71	19.66	5.14
1	75	0.97	1.97	11.33	3.33	25.37	7.20
4	0	0.33	2.94	48	7.92	34.69	18.12
4	75	0.23	2.49	69	9.08	42.65	23.80

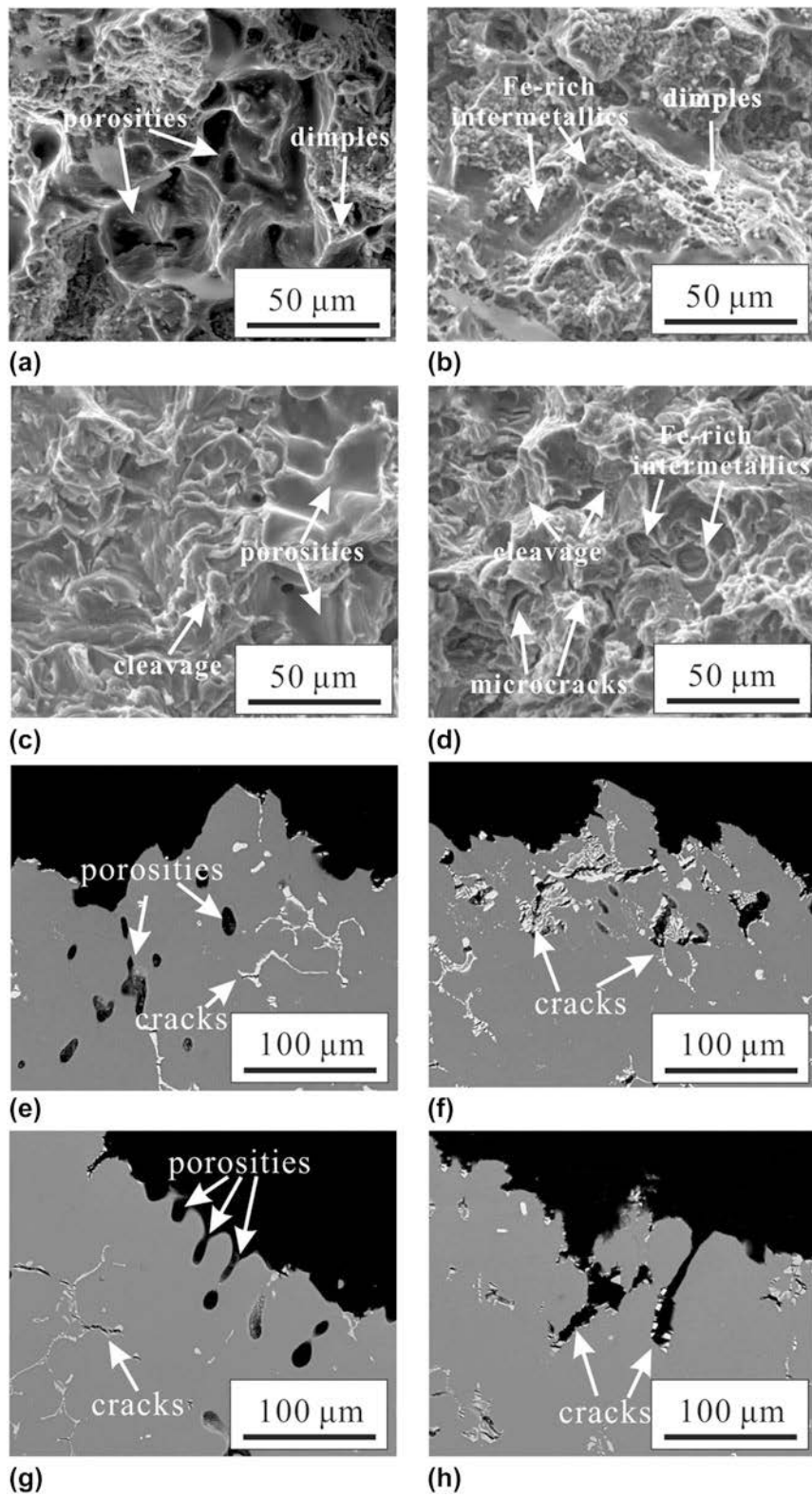


FIG. 8. Fracture surface of heat-treated Al–5.0Cu–0.6Mn alloys with different Si contents and applied pressures: (a) alloy 1 without applied pressure; (b) alloy 1 with 75 MPa applied pressure; (c) alloy 4 without applied pressure; (d) alloy 4 with 75 MPa applied pressure; longitudinal sections near the fracture surfaces: (e) alloy 1 without applied pressure; (f) alloy 1 with 75 MPa applied pressure; (g) alloy 4 without applied pressure; (h) alloy 4 with 75 MPa applied pressure.

about 69% and the number density and dispersoid strengthening increase by at least approximately 734% and 253%, respectively. Thus, it can be deduced that the addition of Si has a great influence on the precipitation of the T phase. Moreover, an increase in the applied pressure from 0 to 75 MPa provides precipitation of the T phase with a smaller equivalent diameter and a higher number density. For example, the equivalent diameter decreased by nearly 9% and the number density and volume fraction of alloy 1 increased by approximately 97% and 40%, respectively, which fully confirms that the applied pressure also plays a major role in the precipitation of the T phase. These indicate that Si addition and applied pressure both promote the formation of the high-density small dispersoids T phase and contribute to the enhancement of yield strength.

The decrease of elongation with Si addition can be concluded from fracture characterization. Figure 8 shows the SEM images of fracture morphology and longitudinal sections near the fracture surfaces of the alloys. It is clear from low Si alloys [Figs. 8(a) and 8(b)] that large numbers of dimples exist at the fracture surface, while many coarse cleavages and microcracks are observed in medium- and high-Si-content alloys [Figs. 8(c) and 8(d)]. These indicate that increasing Si content changes the fracture morphology from being ductile to quasi-cleavage. Moreover, applied pressure is helpful to eliminate porosity. A previous study demonstrated that the detrimental effect of compact α -Fe is less than that of α (CuFe).¹³ However, the increasing volume of α -Fe in the alloys with increasing Si content still results in the decrease of elongation. The longitudinal sections near the fracture surfaces of different alloys are shown in Figs. 8(e)–8(h). It can be seen that large numbers of porosities are observed at the fracture surface in alloys without applied pressure [Figs. 8(e) and 8(g)], which is the site for crack initiation. The cracks usually exist in the coarse Fe-rich intermetallic phases [Figs. 8(f) and 8(h)], indicating that the applied pressure is helpful to eliminate the porosities and hinder crack propagation.

IV. CONCLUSION

The microstructure and mechanical properties of the T5 heat-treated Al–5.0Cu–0.6Mn–0.7Fe alloys with different Si contents produced by GC and SC have been investigated to understand the role of Si in the Fe-rich intermetallic phase formation and their effect on the tensile properties. The main conclusions are as follows:

(1) The increasing Si content increases the volume fraction of Fe-rich intermetallic phases and promotes the formation of α -Fe. With the addition of 0.55% Si in the Al–5.0Cu–0.6Mn–0.7Fe alloy, α -Fe is formed through the eutectoid reaction: $\text{Si} + \text{Al}_6(\text{FeMn}) \rightarrow \alpha\text{-Fe} + \alpha\text{-Al}$; with further increasing the Si content to 1.1%, α -Fe is thermodynamically stable.

(2) The addition of Si in the Al–5.0Cu–0.6Mn–0.7Fe alloy enhances the UTS and YS due to the increasing volume fraction of the T phase, and the less harmful α -Fe has a compact structure, which makes it more difficult for the cracks to initiate and propagate during the tensile test. The increase of the Si content results in fine highly dense T phases; the dispersoid strengthening contributes to the improvement of tensile properties.

(3) The Al–5.0Cu–0.6Mn–0.7Fe alloy with 1.1% Si addition under 75 MP applied pressure shows the best mechanical properties of a UTS of 386 MPa, YS of 280 MPa, and elongation of 8.6%.

ACKNOWLEDGMENTS

The authors would like to acknowledge the financial support from Project (51374110) by the National Natural Science Foundation of China and Project (2015A030312003) by the Natural Science Foundation of Guangdong Province for Research Team. Yuliang Zhao also would like to acknowledge the financial support from Chinese Scholarship Council (CSC).

REFERENCES

1. E. Hornbogen and E.A. Starke, Jr.: Overview no. 102 theory assisted design of high strength low alloy aluminum. *Acta Metall. Mater.* **41**, 1 (1993).
2. Z. Wang, R.T. Qu, S. Scudino, B.A. Sun, K.G. Prashanth, D.V. Louzguine-Luzgin, M.W. Chen, Z.F. Zhang, and J. Eckert: Hybrid nanostructured aluminum alloy with super-high strength. *NPG Asia Mater.* **7**, 1 (2015).
3. J.G. Kaufman and E.L. Rooy: *Aluminum Alloy Castings: Properties, Processes, and Applications* (ASM International, Materials Park, OH, 2004); p. 13.
4. G. Gaustad, E. Olivetti, and R. Kirchain: Improving aluminum recycling: A survey of sorting and impurity removal technologies. *Resour., Conserv. Recycl.* **58**, 79 (2012).
5. J.R. Cui and H.J. Roven: Recycling of automotive aluminum. *Trans. Nonferrous Met. Soc. China* **20**, 2057 (2010).
6. J.A.S. Green: *Aluminum Recycling and Processing for Energy Conservation and Sustainability* (ASM International, Materials Park, OH, 2007); p. 92.
7. US Department of the Interior & US Geological Survey: *Aluminum—Mineral Commodity Summaries 2016* (U.S. Geological Survey, Reston, Virginia, 2016); p. 22.
8. M. Zhang, W.W. Zhang, H.D. Zhao, D.T. Zhang, and Y.Y. Li: Effect of pressure on microstructures and mechanical properties of Al–Cu–based alloy prepared by squeeze casting. *Trans. Nonferrous Met. Soc. China* **17**, 496 (2007).
9. N.A. Belov, A.A. Aksenov, and D.G. Eskin: *Iron in Aluminum Alloys: Impurity and Alloying Element* (CRC Press, London, 2002); p. 1.
10. L.F. Zhang, J.W. Gao, L.N.W. Damaoh, and D.G. Robertson: Removal of iron from aluminum: A review. *Miner. Process. Extr. Metall.* **33**, 99 (2012).
11. Q.L. Zhao, M. Slagsvold, and B. Holmedal: Comparison of the influence of Si and Fe in 99.999% purity aluminum and in commercial-purity aluminum. *Scr. Mater.* **67**, 217 (2012).
12. L.F. Mondolfo: *Aluminum Alloys: Structure and Properties* (Butterworths, London, 1976); p. 8.

13. K. Liu, X. Cao, and X.G. Chen: Tensile properties of Al–Cu 206 cast alloys with various iron contents. *Metall. Mater. Trans. A* **45**, 2498 (2014).
14. K. Liu, X. Cao, and X.G. Chen: Effect of Mn, Si, and cooling rate on the formation of iron-rich intermetallics in 206 Al–Cu cast alloys. *Metall. Mater. Trans. B* **43**, 1231 (2012).
15. H.K. Kamguo, D. Larouche, M. Bourmane, and A. Rahem: Solidification of aluminum–copper B206 alloys with iron and silicon additions. *Metall. Mater. Trans. A* **41**, 2845 (2010).
16. H.K. Kanga, D. Larouche, M. Bourmane, and A. Rahem: Mechanical properties of aluminium–copper B206 alloys with iron and silicon additions. *Int. J. Cast Met. Res.* **25**, 15 (2012).
17. F. Wang, Y.Q. Zeng, B.Q. Xiong, Y.G. Zhang, X.W. Li, Z.H. Li, and H.W. Liu: Effect of Si addition on the microstructure and mechanical properties of Al–Cu–Mg alloy. *J. Alloys Compd.* **585**, 474 (2014).
18. K. Liu, X. Cao, and X.G. Chen: Formation and phase selection of iron-rich intermetallics in Al–4.6Cu–0.5Fe cast alloys. *Metall. Mater. Trans. A* **44**, 682 (2013).
19. K. Liu, X. Cao, and X.G. Chen: Precipitation of iron-rich intermetallic phases in Al–4.6Cu–0.5Fe–0.5Mn cast alloy. *J. Mater. Sci.* **47**, 4290 (2012).
20. W.W. Zhang, B. Lin, D.T. Zhang, and Y.Y. Li: Microstructures and mechanical properties of squeeze cast Al–5.0Cu–0.6Mn alloys with different Fe content. *Mater. Des.* **52**, 225 (2013).
21. W.W. Zhang, B. Lin, J.L. Fan, D.T. Zhang, and Y.Y. Li: Microstructures and mechanical properties of heat-treated Al–5.0Cu–0.5Fe squeeze cast alloys with different Mn/Fe ratio. *Mater. Sci. Eng., A* **588**, 366 (2013).
22. Y.L. Liu, L. Luo, C.F. Han, L.Y. Ou, J.J. Wang, and C.Z. Liu: Effect of Fe, Si and cooling rate on the formation of Fe- and Mn-rich intermetallics in Al–5Mg–0.8Mn alloy. *J. Mater. Sci. Technol.* **32**, 305 (2016).
23. M. Shakiba, N. Parson, and X.G. Chen: Effect of iron and silicon content on the hot compressive deformation behavior of dilute Al–Fe–Si alloys. *J. Mater. Eng. Perform.* **24**, 404 (2015).
24. S.A. El Majid, M. Bamberger, and A. Katsman: *Microstructure and Phase Evolution in A201 Alloys with Additions of Silicon* (Light Metals 2016, TMS, The Minerals, Metals & Materials Society, Nashville, Tennessee 2016); p. 127.
25. H. She, W. Chu, D. Shu, J. Wang, and B.D. Sun: Effects of silicon content on microstructure and stress corrosion cracking resistance of 7050 aluminum alloy. *Trans. Nonferrous Met. Soc. China* **24**, 2307 (2014).
26. D. Mitlin, J.W. Morris, and V. Radmilovic: Catalyzed precipitation in Al–Cu–Si. *Metall. Mater. Trans. A* **31**, 2697 (2000).
27. D.T.L. Alexander and A.L. Greer: Nucleation of the Al₆(Fe,Mn)-to- α -Al-(Fe,Mn)-Si transformation in 3XXX aluminum alloys. I. Roll-bonded diffusion couples. *Philos. Mag.* **84**, 3051 (2004).
28. Y. Li, W. Zhang, H. Zhao, H. You, D. Zhang, M. Shao, and W. Zhang: Research progress on squeeze casting in China. *China Foundry* **11**, 239 (2014).
29. N. Souissi, S. Souissi, J.P. Lecompte, M.B. Amar, C. Bradai, and F. Halouani: Improvement of ductility for squeeze cast 2017 A wrought aluminum alloy using the Taguchi method. *Int. J. Adv. Manuf. Technol.* **78**, 2069 (2015).
30. S.L. Lü, S.S. Wu, L. Wan, and P. An: Microstructure and tensile properties of wrought Al alloy 5052 produced by rheo-squeeze casting. *Metall. Mater. Trans. A* **44**, 2735 (2013).
31. W. Dai, S.S. Wu, S.L. Lü, and C. Lin: Effects of rheo-squeeze casting parameters on microstructure and mechanical properties of AlCuMnTi alloy. *Mater. Sci. Eng., A* **538**, 320 (2012).
32. S.Z. Wang, Z.H. Ji, S. Sumio, and M.L. Hu: Segregation behavior of ADC12 alloy differential support formed by near-liquidus squeeze casting. *Mater. Des.* **65**, 591 (2015).
33. E.A.M. Shalaby, A.Y. Churyumov, A.N. Solonin, and A. Lotfy: Preparation and characterization of hybrid A359/(SiCpSi₃N₄) composites synthesized by stir/squeeze casting techniques. *Mater. Sci. Eng., A* **674**, 18 (2016).
34. Y.X. Liu, W.P. Chen, C. Yang, D.Z. Zhu, and Y.Y. Li: Effects of metallic Ti particles on the aging behavior and the influenced mechanical properties of squeeze-cast (SiCp + Ti)/7075Al hybrid composites. *Mater. Sci. Eng., A* **620**, 190 (2015).
35. C.M. Dinnis, J.A. Taylor, and A.K. Dahle: As-cast morphology of iron-intermetallics in Al–Si foundry alloys. *Scr. Mater.* **53**, 955 (2005).
36. A.M.F. Muggerud, E.A. Mørtzell, Y. Li, and R. Holmestad: Dispersoid strengthening in AA3XXX alloys with varying Mn and Si content during annealing at low temperatures. *Mater. Sci. Eng., A* **567**, 21 (2013).
37. N.Q. Vo, D.C. Dunand, and D.N. Seidman: Improving aging and creep resistance in a dilute Al–Sc alloy by microalloying with Si, Zr, and Er. *Acta Mater.* **63**, 73 (2014).
38. D.T.L. Alexander and A.L. Greer: Solid-state intermetallic phase transformations in 3XXX aluminum alloys. *Acta Mater.* **50**, 2571 (2002).
39. Y.L. Zhao, F.S. Meng, Y. Zhang, D.T. Zhang, C. Yang, and W.W. Zhang: Effect of Si content on microstructures and mechanical properties of Al–5.0Cu–0.6Mn–0.7Fe alloy prepared by squeeze casting. *Chin. J. Nonferrous Met.* **25**, 3041 (2015). (in Chinese).
40. B. Lin, W.W. Zhang, Z.H. Lou, D.T. Zhang, and Y.Y. Li: Comparative study on microstructures and mechanical properties of the heat-treated Al–5.0Cu–0.6Mn– x Fe alloys prepared by gravity die casting and squeeze casting. *Mater. Des.* **59**, 10 (2013).
41. A. Lemieux, J. Langlais, D. Bouchard, and X.G. Chen: Effect of Si, Cu and Fe on mechanical properties of cast semi-solid 206 alloys. *Trans. Nonferrous Met. Soc. China* **20**, 1555 (2010).
42. C.H. Cáceres: Microstructure design and heat treatment selection for casting alloys using the quality index. *J. Mater. Eng. Perform.* **9**, 215 (2000).
43. C.H. Cáceres: A rationale for the quality index of Al–Si–Mg casting alloys. *Int. J. Cast Met. Res.* **10**, 293 (2000).
44. Y.J. Li and L. Arnberg: Quantitative study on the precipitation behavior of dispersoids in DC-cast AA3003 alloy during heating and homogenization. *Acta Mater.* **51**, 3415 (2003).
45. E.A. Brandes and G.B. Brook: *Smithells Metals Reference Book*, 7th ed. (Butterworth-Heinemann Ltd, Oxford, 1992); pp. 22–49.
46. K.E. Knippling, D.C. Dunand, and D.N. Seidman: Criteria for developing castable, creep-resistant aluminum-based alloys—A review. *Z. Metallkd.* **97**, 246 (2006).